Antiferroquadrupole order and magnetic field induced octupole in CeB$_6$

Takeshi Matsumura,[1,2,*] Takumi Yonemura,[1] Keisuke Kunimori,[1] Masafumi Sera,[1,2] Fumitoshi Iga,[3]
Tatsuya Nagao,[4] and Jun-ichi Igarashi[3]

[1]*Department of Quantum Matter, AdSM, Hiroshima University, Higashi-Hiroshima 739-8530, Japan*
[2]*Institute for Advanced Materials Research, Hiroshima University, Higashi-Hiroshima 739-8530, Japan*
[3]*Faculty of Science, Ibaraki University, Mito, Ibaraki 310-8512, Japan*
[4]*Faculty of Engineering, Gunma University, Kiryu, Gunma 376-8515, Japan*

We have studied the antiferroquadrupole ordered phase of CeB$_6$ in magnetic fields by resonant x-ray diffraction. By analyzing the significant change in the energy spectrum on reversing the field direction along [$\bar{1}$ 1 0], we have deduced field dependencies of the antiferro components of magnetic dipole, electric quadrupole, and magnetic octupole moments which are simultaneously induced in the Ce $4f$ orbital with a propagation vector $(\frac{1}{2}, \frac{1}{2}, \frac{1}{2})$. The data treatments are based on theoretically calculated spectral functions. The existence of the field-induced octupole is also concluded for other field directions. We also show direct evidence for the formation of a linear-combination-type antiferroquadrupole order parameter in magnetic fields, which is expressed as $\langle \alpha O_{yz} + \beta O_{zx} + \gamma O_{xy} \rangle$ and changes continuously with the field direction (α, β, γ). A possibility of observing the quadrupolar fluctuation is also pointed out.

PACS number(s): 75.25.Dk, 61.05.cp, 71.27.+a

I. INTRODUCTION

Higher rank multipole moments in f electron systems have recently been recognized as important factors in a rich variety of electronic ordered phases realized at low temperatures.[1,2] When the crystalline electric field (CEF) ground state has a non-Kramers degeneracy, electric quadrupole, magnetic octupole, and even higher rank multipole degrees of freedom can arise. These multipoles may be viewed as an entangled state of spin and orbital degrees of freedom as a result of the strong spin-orbit coupling of the f electrons.

The exchange interaction between higher rank multipoles can be as large as that between magnetic dipole moments. A typical example is the case in CeB$_6$, in which the Ruderman-Kittel-Kasuya-Yosida (RKKY) type exchange interaction is predominant. The RKKY interaction involving spin and orbital degrees of freedom was first studied by Ohkawa so as to be applied to the case of CeB$_6$,[3,4] and was later reformulated by Shiina *et al.* using the concept of multipole moments.[5]

CeB$_6$ crystallizes in the cubic CaB$_6$-type structure (space group $Pm\bar{3}m$, No. 221), where the Ce ion and the B$_6$ octahedral unit form a CsCl-type structure. The CEF ground state is the Γ_8 quartet, and the Γ_7 excited state is well separated at 540 K.[6] CeB$_6$ exhibits two phase transitions at zero field.[7-15] One is an antiferroquadrupole (AFQ) order at $T_Q = 3.3$ K and the other is an antiferromagnetic (AFM) order at $T_N = 2.3$ K.[16,17] One of the anomalous features of these ordered phases is that the AFQ phase is stabilized and T_Q increases in magnetic fields.[9-18] It is now considered that the main origin of this anomalous behavior lies in the antiferro-type interaction between the magnetic octupole moments induced by the magnetic field.[5,19-22] This is well evidenced by the analysis of the NMR line splittings.[12-14,19-23]

Resonant x-ray diffraction (RXD) is a promising probe to observe ordered structures of higher rank multipoles.[24-26] With respect to the observation of the AFQ order in CeB$_6$, several works, including nonresonant diffraction, have already been reported.[27-30] With respect to the field-induced antiferro

octupole (AFO) in the AFQ phase, we have reported that the signal is reflected in the difference of the electric quadrupole ($E2$) resonance intensity on reversing the field direction.[31] We analyzed this asymmetric behavior as caused by the interference between the scatterings from even and odd rank order parameters, and extracted the field dependencies of the AFQ and AFO moments. The significance of the observation by RXD in a different sense from NMR, which probes the transferred hyperfine field at the boron nucleus via the spin polarization of the $2p$ and $2s$ conduction electrons,[32,33] is also described in Ref. 31.

However, our analysis in Ref. 31 remained incomplete because we used the simplest form of the scattering amplitude which does not consider the energy dependence properly. The treatment in Ref. 31 is called the *fast collision approximation*, which is not suited to our case where the interference between different spectral functions is of fundamental importance. This situation is explained in Ref. 34 in detail. The authors have made a spectral analysis based on a more solid theory and gave an explanation to the field reversal effect of the resonance spectrum.

The purpose of the present paper is to analyze the energy spectrum and its field reversal effect using the theory and spectral functions given in Ref. 34. We extract the field dependencies of the AFQ and AFO moments for the field along [$\bar{1}$ 1 0] in the same way as before, but the data treatments are now theoretically more justified. The simultaneously induced AFM dipole is also extracted by analyzing the difference in the electric dipole ($E1$) resonance intensity on the field reversal. The validity of the spectral analysis will be shown also for other field directions. We also show that the AFQ order parameter in magnetic fields can be expressed by a linear combination of $\langle \alpha O_{yz} + \beta O_{zx} + \gamma O_{xy} \rangle$, where α, β, and γ are the direction cosines of the magnetic field. Although this has been theoretically predicted and was indirectly confirmed by the NMR analysis,[20,23] we consider that the direct evidence provided by the present RXD experiment is of great significance.
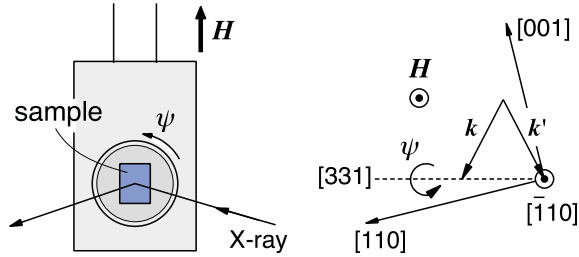
FIG. 1. (Color online) Left: Schematic drawing of the sample rotator inside the superconducting magnet. Right: Scattering geometry in the reciprocal space.

This paper is organized as follows. After describing the experimental procedure in Sec. II, the experimental results and analyses are presented in Sec. III. First, in Sec. III A, we show evidence for the linear-combination-type AFQ order parameter. Next, in Sec. III B, the results of a mean-field model calculation are summarized for reference, which consistently explains the conclusion of Sec. III A. In Sec. III C, we analyze the energy spectra and establish the observation of the AFO moments. The information in Sec. III B will also be useful for a qualitative interpretation of the spectral analysis. Finally, in Sec. IV, we discuss the possibility of observing the quadrupolar fluctuation, evidence for octupolar interaction, and the AFQ order parameters in magnetic fields. The theoretical framework used in the analysis is summarized in the Appendix.

II. EXPERIMENTAL PROCEDURE

A single crystal of CeB_6 was grown by a floating-zone method using an image furnace with four xenon lamps.[35] A slice of the sample with a (331) surface was prepared by spark cutting, and the surface was finally mirror polished. RXD experiments have been performed at beam line 3A of the Photon Factory in the High Energy Accelerator Research Organization (KEK). Magnetic field was applied using a vertical field 8 T superconducting magnet equipped on a two-axis diffractometer. By rotating the sample around the [331] axis using a gear-driven rotator as illustrated in Fig. 1, the azimuthal angle (ψ) can be changed, which simultaneously means the change in the field direction. We define $\psi = 0°$ when $k \times k'$ coincides with the [$\bar{1}$ 1 0] direction. The incident beam was π polarized (electric field $\parallel$ the scattering plane), and the final polarization (σ' or π') was analyzed using a Mo (200) crystal. The measurement was performed around the Ce L_3 absorption edge, where a $2p_{3/2} \leftrightarrow 5d$ resonance ($E1$) or a $2p_{3/2} \leftrightarrow 4f$ resonance ($E2$) occurs. All the data presented in this paper are on the $(\frac{3}{2}, \frac{3}{2}, \frac{1}{2})$ superlattice reflection and the temperature is at 2.5 K in the AFQ phase.

III. RESULTS AND ANALYSIS

A. AFQ order parameter in magnetic fields

We first demonstrate that the AFQ order parameter of CeB_6 in magnetic fields is expressed by a linear combination of $\langle \alpha O_{yz} + \beta O_{zx} + \gamma O_{xy} \rangle$ as has been previously considered through the analysis of NMR line splitting,[20,23] where (α, β, γ) represents the unit vector along the magnetic-field
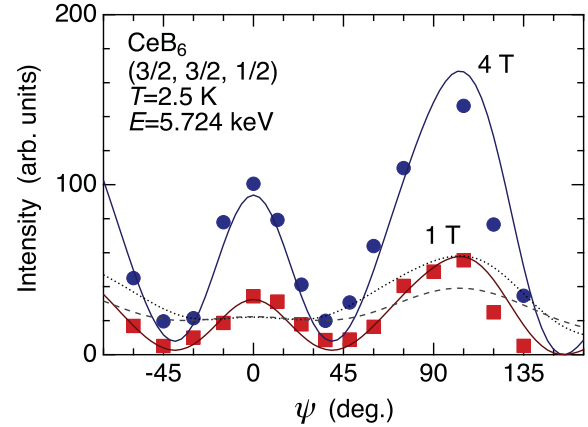

FIG. 2. (Color online) ψ dependencies of the integrated intensity of the $(\frac{3}{2}, \frac{3}{2}, \frac{1}{2})$ reflection at the $E1$ resonance in magnetic fields of 1 T and 4 T without polarization analysis. Solid lines are the intensity curves represented by $|\alpha Z_{yz} + \beta Z_{zx} + \gamma Z_{xy}|^2$, expected for a single-domain linear-combination-type AFQ order. Dotted line shows $|\alpha Z_{yz}|^2 + |\beta Z_{zx}|^2 + |\gamma Z_{xy}|^2$, representing a selected domain state depending on the field direction. Dashed line shows $(|Z_{yz}|^2 + |Z_{zx}|^2 + |Z_{xy}|^2)/3$, representing a three-domain state with equal populations. See text.

direction. This means that the AFQ order parameter changes continuously as a function of the field direction. Although the NMR analysis was performed consistently, it is still of great significance to observe the AFQ order parameter directly by RXD.

Figure 2 shows the ψ dependence of the $E1$ intensity in the AFQ phase in magnetic fields of 1 T and 4 T. The rocking scan was performed at each ψ, and the integrated intensity was normalized by that of the (3, 3, 1) fundamental reflection measured in the same scattering geometry using the $\lambda/2$ contamination in the incident beam. The data points are compared with the calculated curves for three models of the AFQ structure. One is a single-domain linear-combination-type order, where the order parameter is represented by $\langle \alpha O_{yz} + \beta O_{zx} + \gamma O_{xy} \rangle$. In this case, the intensity should be proportional to $|\alpha Z_{yz} + \beta Z_{zx} + \gamma Z_{xy}|^2$, where Z_{yz}, Z_{zx}, and Z_{xy} represent the resonance structure factor $Z_{E1}^{(2)}$ (rank 2, $E1$) for the $\langle O_{yz} \rangle$-, $\langle O_{zx} \rangle$-, and $\langle O_{xy} \rangle$-type AFQ order, respectively. These are shown in Fig. 3. As shown by the solid lines in Fig. 2, the data points for 1 T and 4 T can well be reproduced by this single-domain linear-combination model. Note that both
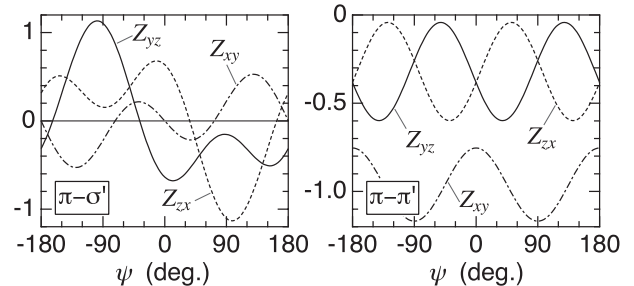

FIG. 3. ψ dependencies of the calculated $Z_{E1}^{(2)}$ parameter (rank 2, $E1$) for the O_{yz}-, O_{zx}-, and O_{xy}-type AFQ ordered state.

π-σ' and π-π' contributions are added because the polarization analysis is not performed.

Another case is that the order parameter is fixed to $\langle O_{yz} \rangle$, $\langle O_{zx} \rangle$, or $\langle O_{xy} \rangle$, and forming domains. When the domain population of each phase is equal to 1/3, the intensity should be proportional to $(|Z_{yz}|^2 + |Z_{zx}|^2 + |Z_{xy}|^2)/3$ as shown by the dashed line. When the domain population changes as a function of the field direction similarly to the case of the single-domain state, the intensity should be proportional to $|\alpha Z_{yz}|^2 + |\beta Z_{zx}|^2 + |\gamma Z_{xy}|^2$ as shown by the dotted line. We can clearly see that these fixed-domain models cannot explain the experimental results.

On the other hand, at zero field, the three-domain state of $\langle O_{yz} \rangle$, $\langle O_{zx} \rangle$, and $\langle O_{xy} \rangle$ with equal populations is presumably realized. The transition from the three-domain state to the single-domain state gives rise to anomalies in physical properties at around 0.1 T.[36,37] The transition is also observed in our RXD experiments as a steep increase in intensity from $H = 0$ to 0.1 T at $\psi = 0°$ and $90°$.[31,38] This change in intensity can be explained as the transition from the dashed line to the solid line shown for 1 T in Fig. 2. The mechanism of this transition will be discussed later.

B. Mean-field calculation

In this subsection, we summarize the field-induced multipoles and the resonance structure factors that are expected from a mean-field calculation. The calculated results are consistent with the experimental result in Sec. III A, and will also be useful in the spectral analysis performed in the next subsection. We assume the following Hamiltonian which has been considered realistic:[20,23,39,40]

$$\mathcal{H} = \sum_i \{ \mathcal{H}_{CEF} - g\mu_B \boldsymbol{J}(i) \cdot \boldsymbol{H} \} - \sum_{i,j} K_{dip} \boldsymbol{J}(i) \cdot \boldsymbol{J}(j)$$

$$- \sum_{i,j} \sum_{\gamma} K_{quad} O_\gamma(i) O_\gamma(j) \quad (\gamma = yz, zx, xy)$$

$$- \sum_{i,j} K_{oct} T_{xyz}(i) T_{xyz}(j), \tag{1}$$

where $\mathcal{H}_{CEF}$ is the cubic CEF giving the Γ_8 ground state. Dipole, quadrupole, and octupole exchange interactions are represented by K_{dip}, K_{quad}, and K_{oct}, respectively. We treated the Hamiltonian in a two-sublattice model. We assumed $K_{dip} = -0.6$ K, $K_{quad} = -2.92$ K, and $K_{oct} = -0.022$ K. With these parameters, $T_Q = 3.3$ K and 4.2 K are obtained for $H = 0$ T and 4 T, respectively.

Figure 4 shows the ψ dependencies of the order parameters at $H = 4$ T and $T = 2.5$ K. Each quadrupole component oscillates sinusoidally, and the linear combination of $\langle \alpha O_{yz} + \beta O_{zx} + \gamma O_{xy} \rangle$ behaves as an antiferro-type order parameter. With the ferromagnetic component $\langle \alpha J_x + \beta J_y + \gamma J_z \rangle$, the antiferro-type order of the $\langle T_{xyz} \rangle$ octupole is always induced almost independently of the field direction.

Once we know the wave function of the Ce ion from the mean-field solution, we can calculate $\langle z_\mu^{(\nu)} \rangle$ in Eqs. (A3) and (A4). Since the geometrical factors $P_\mu^{(\nu)}$ are uniquely determined, we can calculate the resonance structure factors $Z_{E1}^{(\nu)}$ and $Z_{E2}^{(\nu)}$. The calculated ψ dependencies of $Z_{E1}^{(\nu)}$ and $Z_{E2}^{(\nu)}$ for π-σ' and π-π' at $H = 4$ T and $T = 2.5$ K are
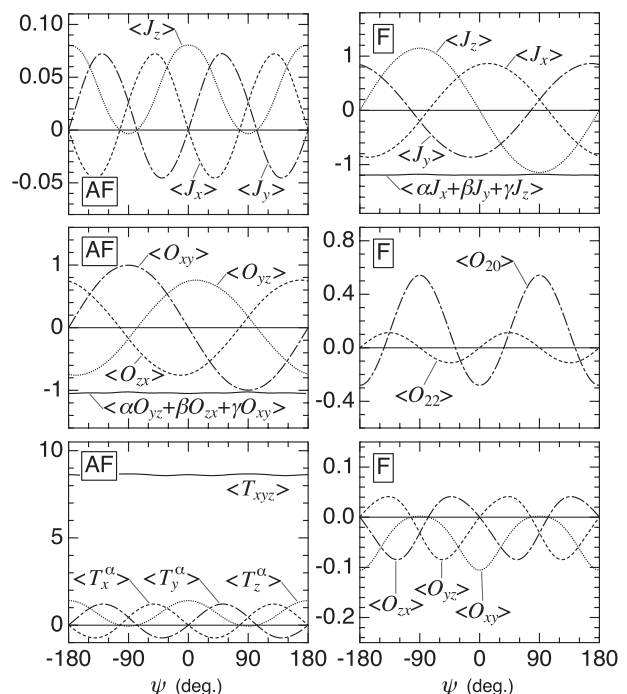

FIG. 4. ψ dependencies of the mean-field solution at $H = 4$ T and $T = 2.5$ K. AF and F represent antiferro and ferro components, respectively.

shown in Fig. 5. It is noted that $Z_{E1}^{(2)}$ can be reproduced by $\alpha Z_{yz} + \beta Z_{zx} + \gamma Z_{xy}$ from Fig. 3. Figure 6 shows the H dependence of the mean-field solution calculated for $\psi = 0°$ and $90°$. The basic features are the same as those reported in Refs. 39 and 40.

C. Spectral analysis

In this subsection, we analyze the energy spectra using the theoretically obtained spectral functions, and assign the origin of the spectral anomalies to specific multipole moments.
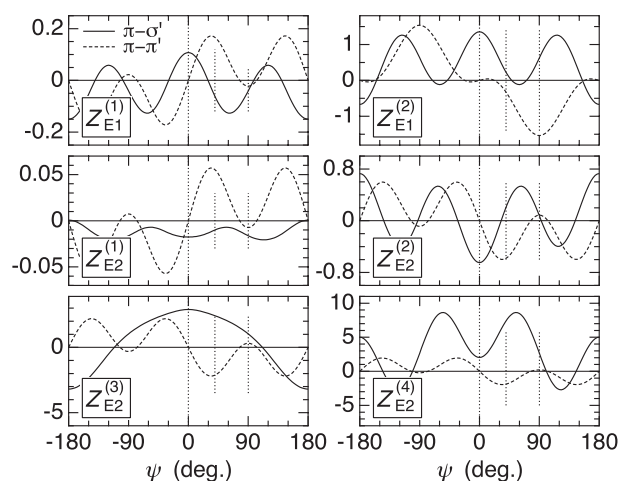

FIG. 5. ψ dependence of the calculated Z parameters for the $(\frac{3}{2}, \frac{3}{2}, \frac{1}{2})$ reflection at $H = 4$ T and $T = 2.5$ K for the mean-field model described in the text. The dotted vertical lines indicate the angle positions where the measurements have been made.
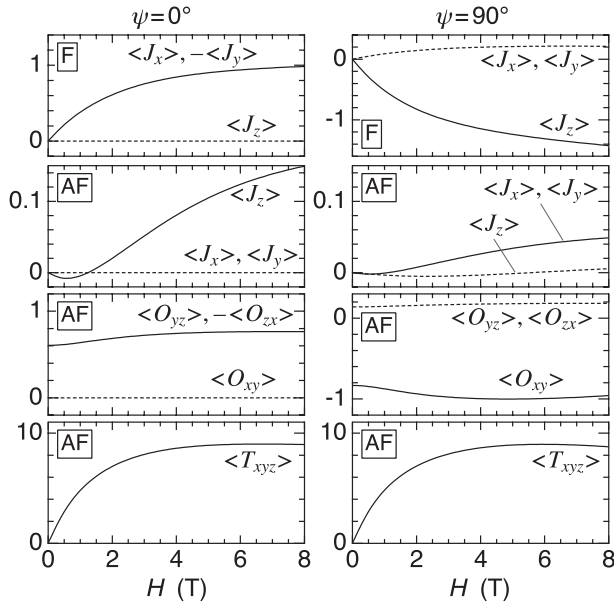
FIG. 6. *H* dependence of the calculated order parameters for the mean-field model described in the text. AF and F represent antiferro and ferro components, respectively.

The intensities were obtained by measuring the rocking curve (ω scan) at each energy and magnetic field. Although the intensities are plotted on an arbitrary scale, they can be compared between the figures.

Energy dependence of the absorption coefficient was deduced from the fluorescence spectrum reported in Ref. 31. It is noted that we used the same absorption coefficient at zero field for all the spectrum in magnetic fields because the field dependence of the absorption coefficient was negligibly small in comparison with the change in intensity of the resonant diffraction. In actuality, the absorption coefficient can be field dependent and can even exhibit dichroism due to a ferro-type ordering of the orbital moments induced by the field. However, we confirmed that the effect was too small to be detected within the present experimental accuracy; therefore, it is not necessary to consider the field dependence of the absorption coefficient in the present analysis.

1. $\psi = 0°$, $H \parallel [-1,1,0]$

In our previous work of Ref. 31, we did not describe the difference in intensity on field reversal at the $E1$ resonance because it was very small below 2 T. In the present work, we have extended the measurement up to ± 6 T and investigated the spectrum in more detail. As pointed out in Ref. 34, the difference term can arise at the $E1$ energy, which is explicitly shown in Eq. (A7). Figure 7 shows the energy spectra at $H = \pm 5$ T. In addition to the difference at the $E2$ resonance as has already been reported in our previous work,[31] we can clearly observe a difference also at the $E1$ resonance. The average and the difference spectra for $H = \pm 5$ T are shown in Fig. 8. Here, we analyze the experimental spectra using the spectral functions of $\alpha_{E1}^{(\nu)}(\omega)$ and $\alpha_{E2}^{(\nu)}(\omega)$ used in Ref. 34, regarding $Z_{E1}^{(\nu)}$ and $Z_{E2}^{(\nu)}$ as experimental parameters.

The situation at $\psi = 0°$ is very simple, and provides us with an ideal condition to extract various significant physical
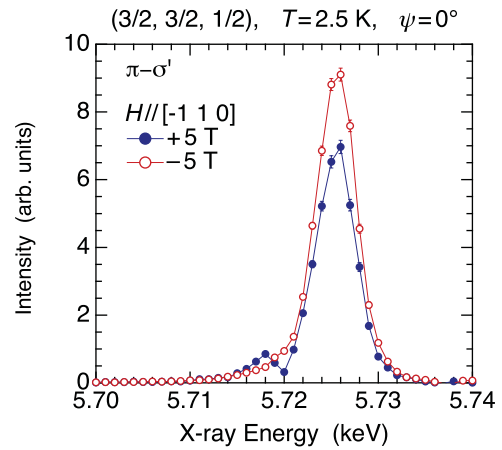

FIG. 7. (Color online) X-ray energy spectra at $H = \pm 5$ T and $\psi = 0°$ after the absorption correction.

parameters. From the mean-field calculation, the antiferro moments induced are $\langle J_z \rangle$, $\langle O_{yz} \rangle = -\langle O_{zx} \rangle$, $\langle T_{xyz} \rangle$, $\langle T_z^\alpha \rangle$, $\langle H_x^\alpha \rangle = \langle H_y^\alpha \rangle$, and $\langle H_x^\beta \rangle = -\langle H_y^\beta \rangle$. With respect to the dipole and quadrupole moments, the above information is supported by the results of neutron diffraction,[17] NMR analysis,[20] and also by our result that the intensity for π-π' channel vanishes. Therefore, we can impose the following restrictions on the rank 1 and rank 2 Z parameters: $Z_{E1}^{(1)}/Z_{E2}^{(1)} = P_{E1,3}^{(1)}/P_{E2,3}^{(1)} = -6.1$ and $Z_{E1}^{(2)}/Z_{E2}^{(2)} = P_{E1,3}^{(2)}/P_{E2,3}^{(2)} = -2.1$. Thus, the six Z parameters are reduced to four. In addition, $P_{E2,4}^{(3)}$, the geometrical factor for $\langle T_z^\alpha \rangle$, is less than 2% compared with
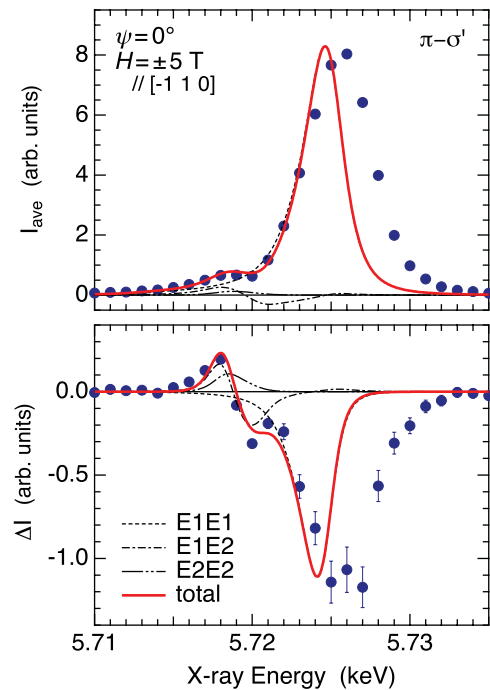

FIG. 8. (Color online) Average and difference spectra for the data in Fig. 7. The solid lines are the fits to the data using the spectral functions used in Ref. 34. The detailed spectral components are also shown by the dotted, single-dotted, and double-dotted lines.

$P_{E2,1}^{(3)}$ for $\langle T_{xyz} \rangle$. Therefore, the contribution to the intensity from $\langle T_z^\alpha \rangle$ can be neglected.

The fitting results are plotted by the lines in Fig. 8. Both $I_{ave}(\omega)$ and $\Delta I(\omega)$ can well be explained by properly choosing the Z parameters. Since the original spectral functions in Ref. 34 do not intend the best fit to the experimental data, there remain differences in the resonance energy and the width. But this is a trivial matter which does not affect our analysis. A few points should be noted. First, the rank-4 contribution to the spectrum was found to be negligibly small. The fitted spectrum hardly depends on $Z_{E2}^{(4)}$. This means that we cannot deduce $Z_{E2}^{(4)}$ properly. Therefore, in the fitting procedure, $Z_{E2}^{(4)}$ was fixed to a value that was reasonably expected from the mean-field calculation. Second, the $(Z_{E1}^{(2)})^2$ term accounts for more than 98% of I_{E1E1}^{ave}, whereas the $(Z_{E1}^{(1)})^2$ term less than 2%. This shows that the $E1$ resonance reflects almost only the AFQ moment. Third, among the four terms of ΔI_{E1E2} in Eq. (A8), the $Z_{E1}^{(2)} Z_{E2}^{(3)}$ term accounts for more than 95% of the total. In the same manner, the $Z_{E2}^{(2)} Z_{E2}^{(3)}$ term accounts for more than 98% of ΔI_{E2E2}.

Therefore, the following approximations are justified:

$$I_{ave}(\omega_1) \approx \left| \alpha_{E1}^{(2)}(\omega_1) \right|^2 \left(Z_{E1}^{(2)} \right)^2, \tag{2}$$

$$\Delta I(\omega_1) \approx 2\text{Im}\left\{ \alpha_{E1}^{*(1)}(\omega_1) \alpha_{E1}^{(2)}(\omega_1) \right\} Z_{E1}^{(1)} Z_{E1}^{(2)}, \tag{3}$$

$$\Delta I(\omega_2) \approx -2\text{Im}\left\{ \alpha_{E1}^{*(2)}(\omega_2) \alpha_{E2}^{(3)}(\omega_2) \right\} Z_{E1}^{(2)} Z_{E2}^{(3)} \\ - 2\text{Im}\left\{ \alpha_{E2}^{*(2)}(\omega_2) \alpha_{E2}^{(3)}(\omega_2) \right\} Z_{E2}^{(2)} Z_{E2}^{(3)}, \tag{4}$$
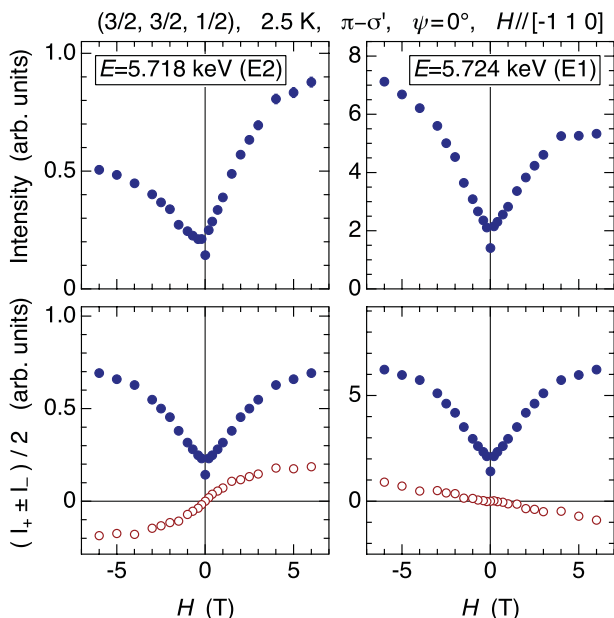

FIG. 9. (Color online) Top: Magnetic-field dependence of the $E2$ (left) and $E1$ (right) resonance intensity. Bottom: Average $(I_{+H} + I_{-H})/2$ (filled circles) and difference $(I_{+H} - I_{-H})/2$ (open circles) components of the intensity for the $E2$ (left) and $E1$ (right) resonances. The jump in intensity at $H = 0.1$ T corresponds to the transition from the three-domain state to the single-domain state described in Sec. III A.
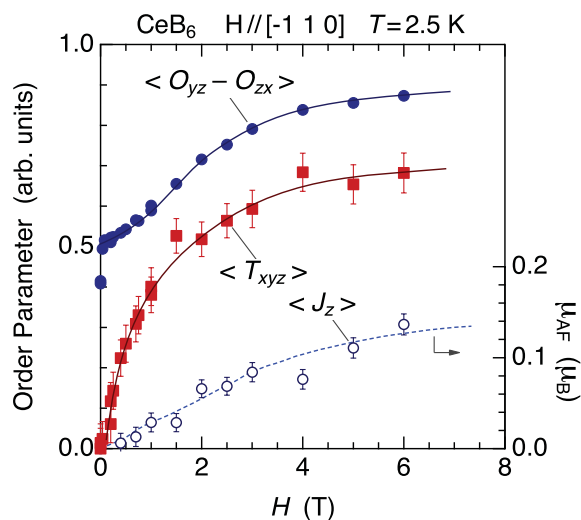

FIG. 10. (Color online) Magnetic-field dependencies of the antiferro-type multipole order parameters of CeB_6 for $H \parallel [\bar{1} 1 0]$ in the AFQ phase at 2.5 K. The dashed line shows the field dependence of the dipole moment measured by neutron diffraction (Ref. 41) whose absolute value was deduced from the NMR analysis (Ref. 23). The solid lines for quadrupole and octupole moments are guides for the eyes.

where $\omega_1 = 5.724$ keV and $\omega_2 = 5.718$ keV. Therefore, $\sqrt{I_{ave}(\omega_1)}$ is proportional to $\langle O_{yz} - O_{zx} \rangle$ and $\Delta I(\omega_1)/\sqrt{I_{ave}(\omega_1)}$ is proportional to $\langle J_z \rangle$. Since $Z_{E1}^{(2)}$ is proportional to $Z_{E2}^{(2)}$, and over 98% of $Z_{E2}^{(3)}$ arises from $\langle T_{xyz} \rangle$ because of the dominant P factor, $\Delta I(\omega_2)/\sqrt{I_{ave}(\omega_1)}$ is proportional to $\langle T_{xyz} \rangle$. Figure 9 shows the experimental results, from which these treatments are performed. The procedure is the same as in Ref. 31, but the field range is extended to ± 6 T.

Figure 10 shows the field dependencies of the multipole order parameters obtained by the above procedure. The scale is arbitrary. With respect to the dipole moment, the absolute antiferromagnetic moment obtained from neutron diffraction and NMR analyses are plotted on an absolute scale.[23,41] The data points of $\langle J_z \rangle$ seem to follow this curve.
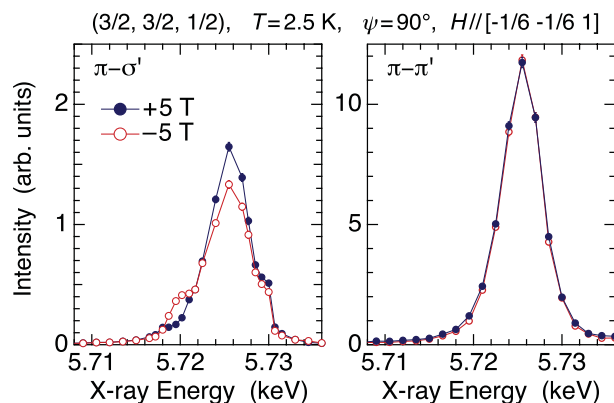

FIG. 11. (Color online) X-ray energy spectra at $H = \pm 5$ T and $\psi = 90°$ for π-σ' and π-π' after the absorption correction.
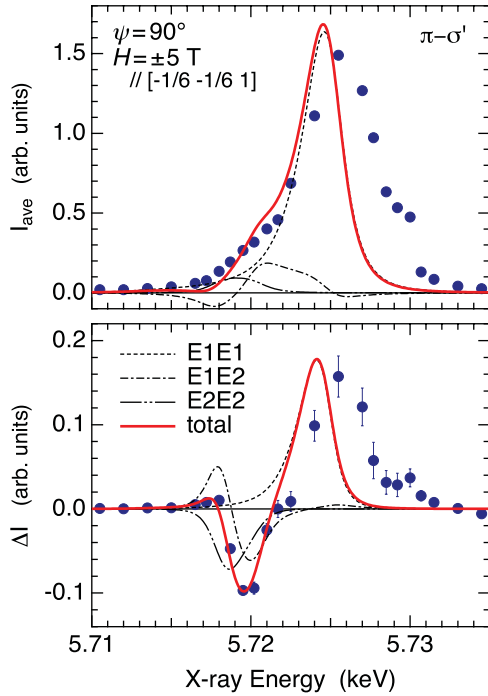
FIG. 12. (Color online) Average and difference spectra for the π-σ' data in Fig. 11. The solid lines are the fits to the data using the spectral functions used in Ref. 34. The detailed spectral components are also shown by the dotted, single-dotted, and double-dotted lines.

2. $\psi = 90°$, $H \parallel [-1/6, -1/6, 1]$

Figure 11 shows the energy spectra at $H = \pm 5$ T and $\psi = 90°$ for the π-σ' and π-π' channels. As shown in the $Z_{E1}^{(2)}$ parameter in Fig. 5, the $E1$ intensity at $E = 5.724$ keV for π-π' is much stronger than that for π-σ'. However, we could hardly observe a field reversal asymmetry in the π-π' channel. The asymmetry was weakly detected in the π-σ' channel. In Fig. 12, we show the average and difference spectra for π-σ'.

We have also tried to fit these spectra using the same spectral functions. The fitting results are shown by the lines in Fig. 12. In spite of the drastic change in the spectrum from that at $\psi = 0°$, especially the appearance of the negative peak at 5.72 keV in ΔI, the whole spectra can well be explained by properly tuning the Z parameters. As for $\psi = 0°$, almost all the contributions to I_{E1E1}^{ave}, ΔI_{E1E2}, and ΔI_{E2E2} were found to be due to the $(Z_{E1}^{(2)})^2$, $Z_{E1}^{(2)} Z_{E2}^{(3)}$, and $Z_{E2}^{(2)} Z_{E2}^{(3)}$ terms, respectively. Because of the change in sign of $Z_{E2}^{(2)}$, which is expected from Fig. 5, ΔI_{E2E2} exhibits a negative peak at 5.718 keV. This peak cancels the positive peak of ΔI_{E1E2} at 5.718 keV, but makes a negative peak apparently at 5.72 keV as a result of the interference with ΔI_{E1E2}. Thus, we can conclude that the antiferro dipole, quadrupole, and octupole moments are induced also in this field direction.

3. $\psi = 40°$, $H \parallel [-1.03, 0.7, 1]$

Figure 13 shows the energy spectra at $H = \pm 5$ T and $\psi = 40°$ for the π-σ' and π-π' channels. As shown in the $Z_{E1}^{(2)}$ parameter in Fig. 5, the $E1$ intensity at $E = 5.724$ keV is much weaker than those for other field directions. This result is consistent with Fig. 2. A very anomalous feature in this
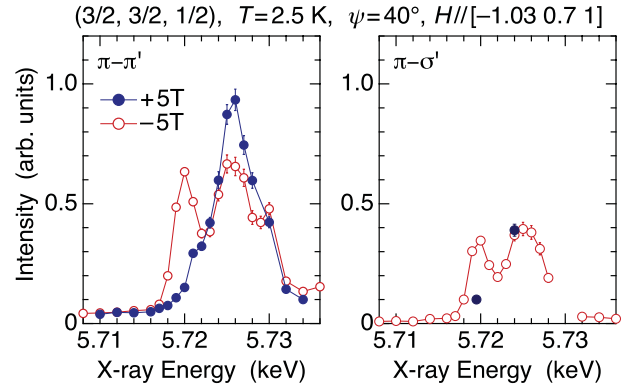

FIG. 13. (Color online) X-ray energy spectra at $H = \pm 5$ T and $\psi = 40°$ for π-π' and π-σ' after the absorption correction.

field direction is that the $E2$ resonance peak appears only for negative fields, which can be observed in Fig. 13. This can be well explained again if we analyze I_{ave} and ΔI using the same spectral functions. The fitting results are shown in Fig. 14. In this case also, the appearance of the negative peak in ΔI at 5.72 keV, in between the $E1$ and $E2$ energies, is a result of the interference between ΔI_{E1E2} and ΔI_{E2E2}.

For $\psi = 90°$ and $40°$, unfortunately, we could not separate the contributions from different kinds of multipole moments because of the complex ingredients of the Z parameters. For these angles, all kinds of multipoles are induced as shown in Fig. 4. Furthermore, the relations with the geometrical P factors do not give simple proportionality as in the case for $\psi = 0°$. We can just mention from the spectral analysis that the quadrupole and octupole moments as large as those at
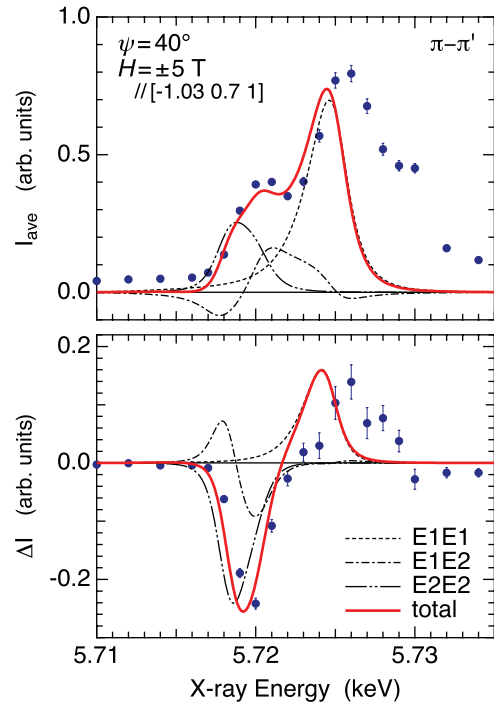

FIG. 14. (Color online) Average and difference spectra for the π-π' data in Fig. 13. The solid lines are the fits to the data using the spectral functions used in Ref. 34. The detailed spectral components are also shown by the dotted, single-dotted, and double-dotted lines.

$\psi = 0°$ are induced also at $\psi = 40°$ and $90°$. More precise, complete, and careful measurements are necessary to extract the detailed order parameters for these angles.

IV. DISCUSSION

A. Quadrupolar fluctuation

We first discuss the field dependencies of the multipole order parameters shown in Fig. 10. With respect to the AFQ and AFO moments, the overall features seem to be consistent with the mean-field calculation shown in Fig. 6. In the single-domain state above 0.1 T, the $\langle O_{yz} - O_{zx} \rangle$ quadrupole increases concavely from a finite value and the $\langle T_{xyz} \rangle$ octupole increases convexly from zero like a Brillouin function. According to the mean-field calculation, the concave increase of $\langle O_{yz} - O_{zx} \rangle$ at low fields is due to the exchange interaction between dipoles competing with the octupolar interaction. If $K_{\text{dip}} = 0$, it increases convexly.

However, it should be noted that the increase of $\langle O_{yz} - O_{zx} \rangle$ from 0.5 to 0.9 in Fig. 10, a nearly 1.8 times increase from the minimum to the maximum, is larger than that expected from the mean-field calculation shown in Fig. 6. This means that $\langle O_{yz} - O_{zx} \rangle$ is more suppressed at low fields. This may be due to the fluctuation of the quadrupolar order parameters which becomes more significant at low fields.[42–44] Figure 4 of Ref. 44 theoretically demonstrates this effect. To establish the existence of quadrupolar fluctuation in CeB$_6$, however, more careful analysis of the H-dependence curve in Fig. 10 is necessary. It is also important to investigate the temperature dependence of the intensity near T_Q more precisely.

On the other hand, it is quite natural that the H dependence of $\langle T_{xyz} \rangle$ behaves like a Brillouin function and seems to follow the mean-field calculation. When we estimate from Fig. 10 the ratio between the AFO and AFQ moments, $\langle T_{xyz} \rangle / \langle O_{yz} - O_{zx} \rangle$, it increases linearly from zero at $H = 0$ T and becomes constant above $H \sim 1.5$ T as shown in Fig. 15. This plot corresponds to Fig. 5 of Ref. 44, which shows that this behavior is universally observed whether the fluctuation exists or not.
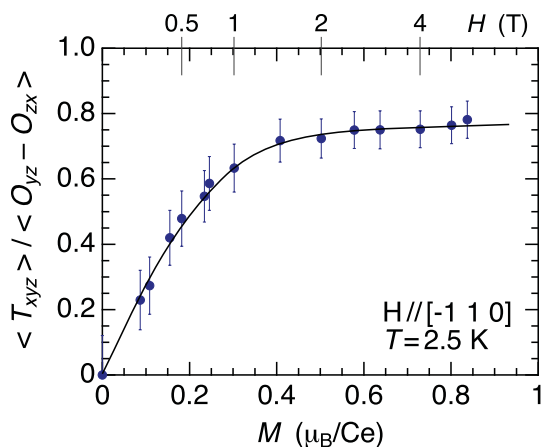

FIG. 15. (Color online) Ratio of the $\langle T_{xyz} \rangle$-AFO to the $\langle O_{yz} - O_{zx} \rangle$-AFQ order parameters for $H \parallel [\bar{1}\,1\,0]$ plotted as a function of uniform magnetization taken from Ref. 10. The units of the vertical axis are arbitrary. The solid line is a guide for the eyes.

The fluctuation effect is less reflected in $\langle T_{xyz} \rangle$, which starts from zero at $H = 0$.

B. Evidence for octupolar interaction

It is noteworthy that the plot of Fig. 15 corresponds well to the plot of Fig. 5 of Ref. 44 for finite values of ε, which represents the deviation of quadrupolar interaction from the SU(4)-symmetric limit. When there is no octupolar interaction, corresponding to the case of $\varepsilon = \infty$, the AFO to AFQ order-parameter ratio becomes proportional to the uniform magnetization. This means that a magnetic field necessarily induces the AFO order on the AFQ order even if there is no AFO interaction. Therefore, the convex curvature of the plot of Fig. 15 is a clear evidence for the existence of the AFO interaction.

C. Quadrupolar order parameter in the AFQ phase

Recently, a reinvestigation of the anisotropy of the AFQ phase has been performed by a magnetostriction measurement.[45] The report questions the AFQ order because no new anisotropic behavior appears in the ordered phase. However, it should be remarked that no anisotropy itself is the essence of the AFQ phase of CeB$_6$ in magnetic fields above 0.1 T. The experimental data reported in Ref. 45 can be understood quite naturally by considering that the AFQ order parameter is expressed as a linear combination of $\langle \alpha O_{yz} + \beta O_{zx} + \gamma O_{xy} \rangle$, which we proved clearly in Sec. III A. As shown in Fig. 4, all the parameters vary continuously with the field direction, keeping constant the uniform magnetization $\langle \alpha J_x + \beta J_y + \gamma J_z \rangle$, AFQ moment $\langle \alpha O_{yz} + \beta O_{zx} + \gamma O_{xy} \rangle$, and the AFO moment $\langle T_{xyz} \rangle$. The single-domain state of the AFQ phase above 0.1 T is quite isotropic. This is an important outcome of the AFO interaction, realizing the easy and continuous reorientation of the AFQ moment. As a result, the ψ dependence of the $\langle O_{20} \rangle$ ferro component shown in Fig. 4, which is related to l/l_0 along [001], is almost the same as that in the paramagnetic phase. The data in Ref. 45 support our present picture of the AFQ phase. With respect to the magnetic susceptibility, anisotropic behavior is clearly observed if one performs the measurement below 0.1 T with domain distributions.[46]

D. Low-field transition in the AFQ phase

The mechanism of the domain motion from the three-domain state at zero field to the single-domain state above 0.1 T may be an important problem. In actuality, the AFQ domain state at zero field is sensitive to subtle external strains, and the actual domain state at the sample surface might not be the three-domain state.[47] Whatever the zero-field AFQ domain state, however, the field dependence of the intensity between 0 T and 0.1 T is worth discussion. If we look at the data at low fields for $H \parallel [\bar{1}\,1\,0]$, which is more clearly shown in Refs. 31 and 38 though without polarization analysis, we notice that the intensity varies linearly from $H = 0$ to the transition field and is continuously connected to the single-domain state with the order parameter $\langle O_{yz} - O_{zx} \rangle / \sqrt{2}$. No discontinuous jump is observed within the experimental accuracy. There also seems no hysteresis.

It should be remarked that the three domains of $\langle O_{yz} \rangle$, $\langle O_{zx} \rangle$, and $\langle O_{xy} \rangle$ have the same intensities at $\psi = 0°$, as is expected from the calculated structure factors in Fig. 3 and also from the dashed and dotted lines in Fig. 2. The linear increase in intensity cannot be explained by considering only the domain redistribution among the three individual domains. It is necessary to consider a gradual increase in the fraction of the $\langle O_{yz} - O_{zx} \rangle / \sqrt{2}$ linear-combination state. A simple scenario may be that the domains at zero field change to the $\langle O_{yz} - O_{zx} \rangle / \sqrt{2}$ state through a domain-wall motion, resulting in a gradual increase in the volume fraction. In this case, weak hysteresis should be observed. Of course, there is a possibility that it was too weak to be detected in our x-ray diffraction experiment.

Another possible scenario is a gradual mixing of the $\langle O_{yz} - O_{zx} \rangle / \sqrt{2}$ component into the zero-field state. If we presume the three-domain state, the order parameter of the $\langle O_{yz} \rangle$ domain, for example, is expressed as $\langle a O_{yz} - b O_{zx} \rangle$, and the coefficient (a,b) changes gradually from $(1,0)$ to $(\frac{1}{\sqrt{2}}, \frac{1}{\sqrt{2}})$. It changes from $(0,1)$ to $(\frac{1}{\sqrt{2}}, \frac{1}{\sqrt{2}})$ in the $\langle O_{zx} \rangle$ domain. The $\langle O_{xy} \rangle$ domain is expressed as $\langle a O_{xy} + b(O_{yz} - O_{zx}) \rangle$, and (a,b) changes from $(1,0)$ to $(0, \frac{1}{\sqrt{2}})$. The gradual mixing of different quadrupole components can be viewed as quadrupole rotation. In the present case of CeB$_6$, the rotation is probably controlled by the energy gain due to the AFO interaction which becomes significant in magnetic fields. The critical field of 0.1 T corresponds to the energy of the AFO interaction to overcome the quadrupole-strain coupling which stabilizes the AFQ domain state at zero field. In addition, the mixing mechanism is not necessarily accompanied by a domain-wall motion. Therefore, a hysteresis may not be observed. In any case, the present experimental data are not sufficient to prove the mechanism of the low-field transition in CeB$_6$. More detailed measurement with polarization analysis is necessary.

Finally, with regard to the AFQ order, the recent discovery of the inelastic resonant peak at $(\frac{1}{2}, \frac{1}{2}, \frac{1}{2})$ by neutron scattering is quite significant.[48] Although the mechanism of the peak has not been clarified, we think that it must be strongly associated with the AFQ order.[49]

V. CONCLUSION

We have studied the AFQ phase of CeB$_6$ in magnetic fields by RXD, where various kinds of higher rank multipole moments are induced. First, we have directly shown that the AFQ order parameter in magnetic fields is expressed by a linear combination of $\langle \alpha O_{yz} + \beta O_{zx} + \gamma O_{xy} \rangle$. This means that the AFQ order parameter rotates continuously as a function of the field direction. Second, we have analyzed the asymmetric behavior of the energy spectrum with respect to the field reversal more systematically than the previous report. The data treatment to extract the multipole moments has been more solidly justified by using the theoretically calculated spectral functions. Thus, the field dependencies of the AFM, AFQ, and AFO ordered moments have been deduced simultaneously for the field direction along $[\bar{1} 1 0]$. A possibility of observing the quadrupolar fluctuation at low fields was pointed out. Finally, from the plot of the AFO to AFQ ratio as a function of

the uniform magnetization, we also pointed out experimental evidence for the AFO interaction.

APPENDIX: THEORETICAL FRAMEWORK

In this section, we briefly review the theoretical framework of Ref. 34 that is necessary to analyze the experimental results. The observed intensity at an x-ray energy $E = \hbar\omega$ is proportional to $|F_{E1}(\omega) + F_{E2}(\omega)|^2$, where F_{E1} and F_{E2} are the resonant scattering amplitudes for the $E1$ and $E2$ processes, respectively. They are expressed as follows:

$$F_{E1}(\omega) = \sum_{\nu=0}^{2} \alpha_{E1}^{(\nu)}(\omega) \sum_{\mu=1}^{2\nu+1} P_{E1,\mu}^{(\nu)}(\boldsymbol{\varepsilon}, \boldsymbol{\varepsilon}') \langle z_\mu^{(\nu)} \rangle, \quad \text{(A1)}$$

$$F_{E2}(\omega) = \frac{k^2}{9} \sum_{\nu=0}^{4} \alpha_{E2}^{(\nu)}(\omega) \sum_{\mu=1}^{2\nu+1} P_{E2,\mu}^{(\nu)}(\boldsymbol{\varepsilon}, \boldsymbol{\varepsilon}', \hat{\boldsymbol{k}}, \hat{\boldsymbol{k}}') \langle z_\mu^{(\nu)} \rangle. \quad \text{(A2)}$$

$z_\mu^{(\nu)}$ is the operator equivalent of the μth component of the rank-ν multipole tensor, which are defined in Table I of Ref. 50. Conventional notations of multipoles such as T_x^α also follow the table. Note that $\langle z_\mu^{(\nu)} \rangle$ for the $(\frac{3}{2}, \frac{3}{2}, \frac{1}{2})$ reflection represents the antiferro component of the expectation value. The ferro component does not contribute to the intensity of the superlattice reflection. $P_{E1,\mu}^{(\nu)}$ and $P_{E2,\mu}^{(\nu)}$ are the geometrical factor of the component μ and rank ν for $E1$ and $E2$ resonances, respectively, which are fully written in Refs. 34 and 50. The most important point in these expressions is that the rank-dependent energy profiles, $\alpha_{E1}^{(\nu)}(\omega)$ and $\alpha_{E2}^{(\nu)}(\omega)$, are explicitly included. This point plays an important role in the analysis.

We write the resonance structure factor as follows:

$$Z_{E1}^{(\nu)} = \sum_{\mu=1}^{2\nu+1} P_{E1,\mu}^{(\nu)}(\boldsymbol{\varepsilon}, \boldsymbol{\varepsilon}') \langle z_\mu^{(\nu)} \rangle, \quad \text{(A3)}$$

$$Z_{E2}^{(\nu)} = \sum_{\mu=1}^{2\nu+1} P_{E2,\mu}^{(\nu)}(\boldsymbol{\varepsilon}, \boldsymbol{\varepsilon}', \hat{\boldsymbol{k}}, \hat{\boldsymbol{k}}') \langle z_\mu^{(\nu)} \rangle. \quad \text{(A4)}$$

By changing the external conditions of temperature, magnetic field, and field direction, $\langle z_\mu^{(\nu)} \rangle$ changes. Another important point in our analysis is that the odd rank tensor changes its sign when the field direction is reversed. The even rank tensors do not change signs with the field reversal. Therefore, the intensity at $+H$ and $-H$ is expressed as

$$I(\omega, \pm H) = \left| \alpha_{E1}^{(2)}(\omega) Z_{E1}^{(2)}(H) + \alpha_{E2}^{(2)}(\omega) Z_{E2}^{(2)}(H) \right.$$
$$+ \alpha_{E2}^{(4)}(\omega) Z_{E2}^{(4)}(H) \pm i \left\{ \alpha_{E1}^{(1)}(\omega) Z_{E1}^{(1)}(H) \right.$$
$$\left. \left. + \alpha_{E2}^{(1)}(\omega) Z_{E2}^{(1)}(H) + \alpha_{E2}^{(3)}(\omega) Z_{E2}^{(3)}(H) \right\} \right|^2. \quad \text{(A5)}$$

Then, the difference and average spectra are expressed as follows:

$$\Delta I(\omega, H) \equiv \{I(\omega, +H) - I(\omega, -H)\}/2$$
$$= \Delta I_{E1E1} + \Delta I_{E1E2} + \Delta I_{E2E2}, \quad \text{(A6)}$$

$$\Delta I_{E1E1} = 2\text{Im}\{\alpha_{E1}^{*(1)}\alpha_{E1}^{(2)}\}Z_{E1}^{(1)}Z_{E1}^{(2)}, \quad \text{(A7)}$$

$$\Delta I_{E1E2} = 2\text{Im}\{\alpha_{E1}^{*(1)}\alpha_{E2}^{(2)}\}Z_{E1}^{(1)}Z_{E2}^{(2)} - 2\text{Im}\{\alpha_{E1}^{*(2)}\alpha_{E2}^{(3)}\}Z_{E1}^{(2)}Z_{E2}^{(3)}$$
$$- 2\text{Im}\{\alpha_{E1}^{*(2)}\alpha_{E2}^{(1)}\}Z_{E1}^{(2)}Z_{E2}^{(1)}$$
$$+ 2\text{Im}\{\alpha_{E1}^{*(1)}\alpha_{E2}^{(4)}\}Z_{E1}^{(1)}Z_{E2}^{(4)}, \quad \text{(A8)}$$

$$\Delta I_{E2E2} = 2\text{Im}\{\alpha_{E2}^{*(1)}\alpha_{E2}^{(2)}\}Z_{E2}^{(1)}Z_{E2}^{(2)} - 2\text{Im}\{\alpha_{E2}^{*(2)}\alpha_{E2}^{(3)}\}Z_{E2}^{(2)}Z_{E2}^{(3)}$$
$$+ 2\text{Im}\{\alpha_{E2}^{*(1)}\alpha_{E2}^{(4)}\}Z_{E2}^{(1)}Z_{E2}^{(4)}$$
$$+ 2\text{Im}\{\alpha_{E2}^{*(3)}\alpha_{E2}^{(4)}\}Z_{E2}^{(3)}Z_{E2}^{(4)}. \quad \text{(A9)}$$

$$I_{\text{ave}}(\omega, H) \equiv \{I(\omega, +H) + I(\omega, -H)\}/2$$
$$= I_{E1E1}^{\text{ave}} + I_{E1E2}^{\text{ave}} + I_{E2E2}^{\text{ave}}, \quad \text{(A10)}$$

$$I_{E1E1}^{\text{ave}} = \left|\alpha_{E1}^{(1)}\right|^2 \left(Z_{E1}^{(1)}\right)^2 + \left|\alpha_{E1}^{(2)}\right|^2 \left(Z_{E1}^{(2)}\right)^2, \quad \text{(A11)}$$

$$I_{E1E2}^{\text{ave}} = 2\text{Re}\{\alpha_{E1}^{*(1)}\alpha_{E2}^{(1)}\}Z_{E1}^{(1)}Z_{E2}^{(1)} + 2\text{Re}\{\alpha_{E1}^{*(2)}\alpha_{E2}^{(2)}\}Z_{E1}^{(2)}Z_{E2}^{(2)}$$
$$+ 2\text{Re}\{\alpha_{E1}^{*(1)}\alpha_{E2}^{(3)}\}Z_{E1}^{(1)}Z_{E2}^{(3)} + 2\text{Re}\{\alpha_{E1}^{*(2)}\alpha_{E2}^{(4)}\}Z_{E1}^{(2)}Z_{E2}^{(4)},$$
$$\text{(A12)}$$

$$I_{E2E2}^{\text{ave}} = \left|\alpha_{E2}^{(1)}\right|^2 \left(Z_{E2}^{(1)}\right)^2 + \left|\alpha_{E2}^{(2)}\right|^2 \left(Z_{E2}^{(2)}\right)^2 + \left|\alpha_{E2}^{(3)}\right|^2 \left(Z_{E2}^{(3)}\right)^2$$
$$+ \left|\alpha_{E2}^{(4)}\right|^2 \left(Z_{E2}^{(4)}\right)^2 + 2\text{Re}\{\alpha_{E2}^{*(1)}\alpha_{E2}^{(3)}\}Z_{E2}^{(1)}Z_{E2}^{(3)}$$
$$+ 2\text{Re}\{\alpha_{E2}^{*(2)}\alpha_{E2}^{(4)}\}Z_{E2}^{(2)}Z_{E2}^{(4)}. \quad \text{(A13)}$$

It is of essential importance to consider different spectral functions for different rank multipoles. Otherwise, the ΔI_{E1E1} and ΔI_{E2E2} terms vanish, and the experimental data can never be explained.

*tmatsu@hiroshima-u.ac.jp

[1] Y. Kuramoto, H. Kusunose, and A. Kiss, J. Phys. Soc. Jpn. **78**, 072001 (2009).

[2] P. Santini, S. Carretta, G. Amoretti, R. Caciuffo, N. Magnani, and G. H. Lander, Rev. Mod. Phys. **81**, 807 (2009).

[3] F. J. Ohkawa, J. Phys. Soc. Jpn. **52**, 3897 (1983).

[4] F. J. Ohkawa, J. Phys. Soc. Jpn. **54**, 3909 (1985).

[5] R. Shiina, H. Shiba, and P. Thalmeier, J. Phys. Soc. Jpn. **66**, 1741 (1997).

[6] E. Zirngiebl, B. Hillebrands, S. Blumenroder, G. Guntherodt, M. Loewenhaupt, J. M. Carpenter, K. Winzer, and Z. Fisk, Phys. Rev. B **30**, 4052 (1984).

[7] K. N. Lee and B. Bell, Phys. Rev. B **6**, 1032 (1972).

[8] K. Winzer and W. Felsch, J. Phys. (Paris) **39**, C6-832 (1978).

[9] T. Fujita, M. Suzuki, T. Komatsubara, S. Kunii, T. Kasuya, and T. Ohtsuka, Solid State Commun. **35**, 569 (1980).

[10] M. Kawakami, S. Kunii, T. Komatsubara, and T. Kasuya, Solid State Commun. **36**, 435 (1980).

[11] A. Takase, K. Kojima, T. Komatsubara, and T. Kasuya, Solid State Commun. **36**, 461 (1980).

[12] M. Kawakami, S. Kunii, K. Mizuno, M. Sugita, T. Kasuya, and K. Kume, J. Phys. Soc. Jpn. **50**, 432 (1981).

[13] M. Kawakami, H. G. Bohn, H. Lutgemeier, S. Kunii, and T. Kasuya, J. Magn. Magn. Mater. **31-34**, 415 (1983).

[14] M. Takigawa, H. Yasuoka, T. Tanaka, and Y. Ishizawa, J. Phys. Soc. Jpn. **52**, 728 (1983).

[15] N. Sato, S. Kunii, I. Oguro, T. Komatsubara, and T. Kasuya, J. Phys. Soc. Jpn. **53**, 3967 (1984).

[16] J. M. Effantin, J. Rossat-Mignod, P. Burlet, H. Bartholin, S. Kunii, and T. Kasuya, J. Magn. Magn. Mater. **47-48**, 145 (1985).

[17] W. A. C. Erkelens, L. P. Regnault, P. Burlet, J. Rossat-Mignod, S. Kunii, and T. Kasuya, J. Magn. Magn. Mater. **63-64**, 61 (1987).

[18] R. G. Goodrich, D. P. Young, D. Hall, L. Balicas, Z. Fisk, N. Harrison, J. B. Betts, A. Migliori, F. M. Woodward, and J. W. Lynn, Phys. Rev. B **69**, 054415 (2004).

[19] O. Sakai, R. Shiina, H. Shiba, and P. Thalmeier, J. Phys. Soc. Jpn. **66**, 3005 (1997).

[20] R. Shiina, O. Sakai, H. Shiba, and P. Thalmeier, J. Phys. Soc. Jpn. **67**, 941 (1998).

[21] H. Shiba, O. Sakai, and R. Shiina, J. Phys. Soc. Jpn. **68**, 1988 (1999).

[22] O. Sakai, R. Shiina, H. Shiba, and P. Thalmeier, J. Phys. Soc. Jpn. **68**, 1364 (1999).

[23] S. Tsuji, M. Sera, and K. Kojima, J. Phys. Soc. Jpn. **70**, 41 (2001).

[24] J. P. Hannon, G. T. Trammell, M. Blume, and D. Gibbs, Phys. Rev. Lett. **61**, 1245 (1988).

[25] J. P. Hill and D. F. McMorrow, Acta Crystallogr. Sect. A **52**, 236 (1996).

[26] S. W. Lovesey, E. Balcar, K. S. Knight, and J. Fernandez Rodriguez, Phys. Rep. **411**, 233 (2005).

[27] H. Nakao, K. Magishi, Y. Wakabayashi, Y. Murakami, K. Koyama, K. Hirota, Y. Endoh, and S. Kunii, J. Phys. Soc. Jpn. **70**, 1857 (2001).

[28] F. Yakhou, V. P. Plakhty, H. Suzuki, S. V. Gavrilov, P. Burlet, L. Paolasini, C. Vettier, and S. Kunii, Phys. Lett. A **285**, 191 (2001).

[29] Y. Tanaka, U. Staub, K. Katsumata, S. W. Lovesey, J. E. Lorenzo, Y. Narumi, V. Scagnoli, S. Shimomura, Y. Tabata, Y. Onuki, Y. Kuramoto, A. Kikkawa, T. Ishikawa, and H. Kitamura, Europhys. Lett. **68**, 671 (2004).

[30] Y. Tanaka, K. Katsumata, S. Shimomura, and Y. Onuki, J. Phys. Soc. Jpn. **74**, 2201 (2005).

[31] T. Matsumura, T. Yonemura, K. Kunimori, M. Sera, and F. Iga, Phys. Rev. Lett. **103**, 017203 (2009).

[32] K. Hanzawa, J. Phys. Soc. Jpn. **69**, 510 (2000).

[33] K. Hanzawa, J. Phys. Soc. Jpn. **69**, 2121 (2000).

[34] T. Nagao and J. I. Igarashi, Phys. Rev. B **82**, 024402 (2010).

[35] F. Iga, N. Shimizu, and T. Takabatake, J. Magn. Magn. Mater. **177-181**, 337 (1998).

[36] S. Nakamura, T. Goto, and S. Kunii, J. Phys. Soc. Jpn. **64**, 3941 (1995).

[37]N. B. Brandt, V. V. Moschalkov, S. N. Pashkevich, M. G. Vybornov, M. V. Semenov, T. N. Kolobyanina, E. S. Konovalova, and Yu. B. Paderno, Solid State Commun. **56**, 937 (1985).

[38]T. Matsumura, T. Yonemura, K. Kunimori, M. Sera, and F. Iga, J. Phys. Soc. Jpn. **80**, SA054 (2011).

[39]M. Sera and S. Kobayashi, J. Phys. Soc. Jpn. **68**, 1664 (1999).

[40]M. Sera, H. Ichikawa, T. Yokoo, J. Akimitsu, M. Nishi, K. Kakurai, and S. Kunii, Phys. Rev. Lett. **86**, 1578 (2001).

[41]J. Rossat-Mignot, in *Methods of Experimental Physics*, edited by K. Skold and D. L. Price (Academic Press, New York, 1987), Vol. 23C, p. 69.

[42]G. Uimin, Y. Kuramoto, and N. Fukushima, Solid State Commun. **97**, 595 (1996).

[43]N. Fukushima and Y. Kuramoto, J. Phys. Soc. Jpn. **67**, 2460 (1998).

[44]R. Shiina, J. Phys. Soc. Jpn. **70**, 2746 (2001).

[45]M. Amara and R.-M. Galéra, Phys. Rev. Lett. **108**, 026402 (2012).

[46]M. Sera (unpublished).

[47]U. Staub, Y. Tanaka, K. Katsumata, A. Kikkawa, Y. Kuramoto, and Y. Onuki, J. Phys.: Condens. Matter **18**, 11007 (2006).

[48]G. Friemel, Y. Li, A. V. Dukhnenko, N. Yu. Shitsevalova, N. E. Sluchanko, A. Ivanov, V. B. Filipov, B. Keimer, and D. S. Inosov, e-print arXiv:1111.4151.

[49]A. Akbari and P. Thalmeier, Phys. Rev. Lett. **108**, 146403 (2012).

[50]T. Nagao and J. I. Igarashi, Phys. Rev. B **74**, 104404 (2006).